Thermoelectric effects in a strongly correlated model for Na_xCoO_2

Michael R. Peterson,* B. Sriram Shastry, and Jan O. Haerter
Physics Department, University of California, Santa Cruz, California 95064, USA
(Received 6 June 2007; published 18 October 2007)

Thermal response functions of strongly correlated electron systems are of appreciable interest to the larger scientific community both theoretically and technologically. Here, we focus on the infinitely correlated *t-J* model on a geometrically frustrated two-dimensional triangular lattice. Using exact diagonalization on a finite sized system, we calculate the dynamical thermal response functions in order to determine the thermopower, Lorenz number, and dimensionless figure of merit. The dynamical thermal response functions are compared to the infinite frequency limit and shown to be very weak functions of frequency, hence, establishing the validity of the high frequency formalism recently proposed by Shastry [Phys. Rev. B **73**, 085117 (2006)] for the thermopower, Lorenz number, and the dimensionless figure of merit. Further, the thermopower is demonstrated to have a low to intermediate temperature enhancement when the sign of the hopping parameter t is switched from positive to negative for the geometrically frustrated lattice [A. P. Ramirez, in More Is Different, edited by N. P. Org and R. N. Bhatt (Princeton University Press, New Jersey, 2001), p. 255] considered.

DOI: 10.1103/PhysRevB.76.165118 PACS number(s): 72.15.Jf, 65.90.+i, 71.27.+a

I. INTRODUCTION

There is current interest in the physics as well as industrial and engineering communities regarding thermoelectrics of strongly correlated electron systems. This interest has been recently revived by the demonstration of the unexpectedly high thermopower seen in the very interesting material sodium cobalt oxide[1–3] (NCO). Theoretically, thermoelectrics have been a long standing problem in physics especially when concerned with strongly correlated systems which are not amenable to perturbative treatments.

Essentially, there are two standard theoretical approaches concerning the problem of thermoelectrics (see Refs. 4–7). The first makes use of Boltzmann theory often complemented with standard Fermi liquid theory. This methodology is reliable for weakly coupled problems where long lived quasiparticles remain well defined and where perturbation theory remains valid. The second approach is to use the full rigor of the Kubo formalism which is valid for all situations but whose dynamical character makes it unyielding and difficult to make any real progress, especially for strongly correlated systems.

Recently, Shastry[8–10] has proposed a third method which handles the strong electron interactions with the respect which they deserve while avoiding the complexity of the full dynamics of the Kubo formalism. Very briefly, this methodology considers the ultimate quantities one is usually interested in when calculating conductivities. Often, there is more interest in certain combinations of conductivities, which form more experimentally accessible quantities (such as the thermopower or Seebeck coefficient, Lorenz number, dimensionless figure of merit, the Hall coefficient, etc.), than in the conductivities (electrical, thermal, etc.) themselves. The basic proposal is that certain combinations of conductivities have weak dynamical character (weak frequency dependence), and thus lend themselves to a high frequency expansion. The upshot of this expansion is that it yields formulas that are much simpler, although nontrivial, than the Kubo formulas and yet the interactions are fully respected compared to the usual approximations which risk missing important effects.

Nearly 15 years previously, this basic high frequency expansion methodology was originally employed by Shastry *et al.*[11] to calculate the Hall coefficient (at high temperatures) for a strongly correlated electron model (*t-J* model) with success. In the last year, the present authors[12,13] have applied this high frequency expansion to calculate the Hall coefficient and thermopower for the very interesting NCO system explaining in both quantitative and qualitative detail the physics of the so-called Curie-Weiss metal for Na_xCoO_2 at electron doping $x \sim 0.7$. This Curie-Weiss metal displays behavior that is an interesting hybrid between those of insulating and metallic systems. The high frequency formalism allowed the investigation of this complicated system successfully by incorporating the important effects of interactions.

Interestingly, Shastry, via the high frequency expansion, was able to predict a low to intermediate temperature thermopower enhancement due to a change in sign of the hopping parameter t of the *t-J* model for a geometrically frustrated[14] two-dimensional triangular lattice.[8,9] This corresponds to a fiduciary hole doped CoO_2 layer of NCO that has yet to be realized experimentally. The lattice topology plays a crucial role in this enhancement as it owes its existence primarily to electron transport and is not thermodynamic or entropic in origin. This prediction was put on firmer footing by the present authors in Ref. 12 concerning the Curie-Weiss metallic phase of NCO which itself has an underlying two-dimensional triangular lattice. We emphasize that we work with a hole doped system ($0 \leqslant n \leqslant 1$, n electron density), and in order to compare with experiments on NCO, we perform a suitable particle-hole transformation.[8,9,12,13]

In this work, we establish the validity and accuracy of the high frequency formalism for the thermopower, Lorenz number, and figure of merit for the strongly correlated electron *t-J* model on a two-dimensional triangular lattice. This is accomplished by comparing the high frequency expressions with those obtained via the full Kubo formalism. This comparison for a strongly correlated system, such as our model,

is only possible through numerical exact diagonalization of a relatively small system ($\mathcal{L}=12$ site lattice). However, we feel that our results provide a much desired and important benchmark for the high frequency formalism establishing its effectiveness and usefulness.

Furthermore, the t-J model is generally representative of strongly correlated electron models so our results should be applicable to other strong correlation models such as the Hubbard model for large U. While the geometrically frustrated triangular lattice provides an interesting enhancement of the thermopower for intermediate temperatures, the general validity of our results should obtain for other lattice topologies (frustrated and nonfrustrated).

The plan of this paper is as follows: In Sec. II, we describe the details of our model and the exact diagonalization used. Section III generally quotes the Kubo formulas for the considered conductivities and the high frequency formulas from Shastry.[8,9] In Secs. IV–VI, we report results for the thermopower (for both positive and negative hopping t), the Lorenz number, and the figure of merit (both for positive hopping $t>0$), respectively. Section VII concludes, while some formulas are given for completeness in the Appendix.

II. t-J MODEL AND DIAGONALIZATION

As mentioned above, we study the t-J model Hamiltonian which describes a strongly correlated hole doped Mott insulator. The Hamiltonian is

$$\hat{H} = -\sum_{\vec{r}\vec{\eta}\sigma} t(\vec{\eta})\tilde{c}^{\dagger}_{\vec{r}+\vec{\eta}\sigma}\tilde{c}_{\vec{r}\sigma} + \frac{1}{2}\sum_{\vec{r}\vec{\eta}} J(\vec{\eta})\vec{S}_{\vec{r}}\cdot\vec{S}_{\vec{r}+\vec{\eta}}, \tag{1}$$

where $\tilde{c}^{\dagger}_{\vec{r}\sigma}(\tilde{c}_{\vec{r}\sigma})=\hat{P}_G c^{\dagger}_{\vec{r}\sigma}(c_{\vec{r}\sigma})\hat{P}_G$ are Gutzwiller projected fermion creation (destruction) operators where the projection operator $\hat{P}_G$ projects out all doubly occupied lattice sites. The lattice vector $\vec{\eta}$ connects nearest neighbors which are coupled [with strength $J(\vec{\eta})$] via their spin degree of freedom ($\vec{S}_{\vec{r}}$ is the three-component spin operator). For simplicity, we take the hopping $t(\vec{\eta})=t$ and spin $J(\vec{\eta})=J$ coupling parameters to be constants and the lattice constant has been set to unity.

In this work, we also aim to apply our calculations to the experimental system of NCO which is electron doped and has been previously modeled using the t-J model.[12,15–17] We use the symmetry of the Hubbard model with regard to half filling to map our system to NCO, i.e., we apply the replacement rules $t\rightarrow -t$, doping $x=|1-n|$, and $q_e\rightarrow -q_e$, where n is electron density per site and $q_e=-|e|$ is the electron charge. At this point, we will abandon referencing particular systems by the electron density and instead reference them by the doping $x\equiv n-1$.

Thermodynamics will be considered within the canonical ensemble, and considering that the goal of this paper is to calculate full thermodynamic Kubo formulas, it is a prerequisite that we obtain the full eigenspectrum of the system in order to calculate all relevant current matrix elements. Therefore, we make progress through the exact numerical diagonalization of a finite system. At this level of study, various approximations such as the finite temperature Lanczos method,[18] dynamical mean field theory,[19] etc., could perhaps muddy the issue of comparing the high frequency expansion of various thermoelectric properties to their full Kubo formulations and, hence, will not be considered. Further, we are interested in the behavior of the system over a whole range of densities and do not wish to confuse the results by considering a smattering of small system sizes along with their particular inherent and unavoidable finite size effects. Therefore, we find that the largest two-dimensional lattice that we can fully diagonalize in a satisfactory way is an $\mathcal{L}=12$ site toroidal lattice (see Fig. 1). Another reason for using this lattice is that it was used extensively in the present authors' previous works[12,13] on the two-dimensional triangular lattice t-J model applied to NCO.

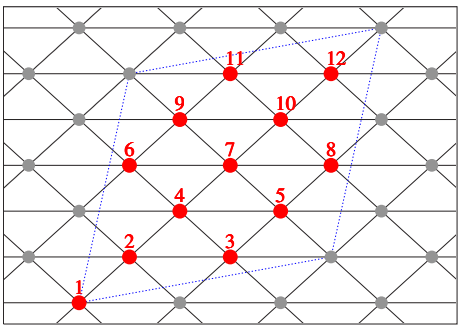

FIG. 1. (Color online) $\mathcal{L}=12$ site torus geometry used throughout this work. We diagonalize the Hamiltonian at all densities of this lattice for the t-J model; however, as explained in the text, we label the electron densities in terms of hole doping x.

To reduce the computational demand of the exact diagonalization to a more manageable size, we employ a number of symmetries. First, we consider only the largest S_z sector of the full Hilbert space, i.e., the smallest $|S_z|$ subspace which is $|S_z|=0$ $(\hbar/2)$ for even (odd) number of electrons. This sector of the full Hilbert space dominates the physics so this "approximation" is as good as exact.[20] The most useful symmetry employed is translational invariance which essentially reduces the Hilbert space dimension by a factor of $\mathcal{L}$. Our largest Hilbert space dimension occurs for $x=1/3$ corresponding to 34 650 states in the $|S_z|=0$ subspace, and after applying translational symmetry, we need only diagonalize matrices of dimension $\sim$2900. While this matrix dimension is not particularly huge in the realm of matrix diagonalization, we must consider a double sum over these $\sim$2900 states to calculate the Kubo formulas. This double sum is quite time consuming and limits our abilities to consider larger lattices and, in fact, it limits our abilities to consider all doping values x on the chosen $\mathcal{L}=12$ site lattice used here. The dopings where we can calculate the full Kubo formula are limited to $x>0.5$ and $x<0.2$.

III. DYNAMICAL THERMAL RESPONSE FUNCTIONS

In this section, we quote the formulas for the Kubo linear response for thermoelectrics following very closely the work of Shastry.[8–10] In particular, we are interested in the electrical

$\sigma(\omega,T)$, thermoelectrical $\gamma(\omega,T)$, and the thermal $\kappa(\omega,T)$ conductivities, respectively. In terms of these conductivities, the ultimate goal of this work are commonly measured physical quantities of interest such as the thermopower S, the Lorenz number L, and the dimensionless figure of merit ZT commonly defined[4,6,7] as

$$S(\omega,T)=\frac{\gamma(\omega,T)}{\sigma(\omega,T)}, \tag{2}$$

$$L(\omega,T)=\frac{\kappa(\omega,T)}{T\sigma(\omega,T)}-\{S(\omega,T)\}^2, \tag{3}$$

and

$$Z(\omega,T)T=\frac{\{S(\omega,T)\}^2}{L(\omega,T)}. \tag{4}$$

These conductivities all have familiar Kubo formulas which, in the Lehmann representation, are written as

$$\sigma(\omega_c,T)=\frac{i}{\hbar\omega_c\mathcal{L}}\left[\langle\hat{\tau}_{xx}\rangle+\frac{\hbar}{\mathcal{Z}}\sum_{n,m}\frac{e^{-\beta\varepsilon_n}-e^{-\beta\varepsilon_m}}{\varepsilon_n-\varepsilon_m+\hbar\omega_c}|\langle n|\hat{J}_x|m\rangle|^2\right], \tag{5}$$

$$\gamma(\omega_c,T)=\frac{i}{\hbar\omega_c T\mathcal{L}}\left[\langle\hat{\Phi}_{xx}\rangle+\frac{\hbar}{\mathcal{Z}}\sum_{n,m}\frac{e^{-\beta\varepsilon_n}-e^{-\beta\varepsilon_m}}{\varepsilon_n-\varepsilon_m+\hbar\omega_c}\langle n|\hat{J}_x|m\rangle\times\langle m|\hat{J}_x^Q|n\rangle\right], \tag{6}$$

and

$$\kappa(\omega_c,T)=\frac{i}{\hbar\omega_c T\mathcal{L}}\left[\langle\hat{\Theta}_{xx}\rangle+\frac{\hbar}{\mathcal{Z}}\sum_{n,m}\frac{e^{-\beta\varepsilon_n}-e^{-\beta\varepsilon_m}}{\varepsilon_n-\varepsilon_m+\hbar\omega_c}|\langle n|\hat{J}_x^Q|m\rangle|^2\right]. \tag{7}$$

In the above, $|k\rangle$ is a normalized eigenstate of the Hamiltonian with energy ε_k, $\mathcal{Z}=\Sigma_k\exp(-\beta\varepsilon_k)$ is the canonical partition function, and $\beta=1/k_BT$ is the inverse temperature. A thermal average is indicated by $\langle\cdots\rangle$. The dynamical temperature variation is turned on adiabatically from the infinite past, i.e., $\omega_c=\omega+i0^+$.

In Eqs. (5)–(7), the charge current $\hat{J}_x$ is formally given by

$$\hat{J}_x=-\lim_{k_x\to 0}\frac{d}{dk_x}[\hat{K}(k_x),q_e\hat{n}(-k_x)], \tag{8}$$

while the heat current $\hat{J}_x^Q$ is

$$\hat{J}_x^Q=-\lim_{k_x\to 0}\frac{1}{2}\frac{d}{dk_x}[\hat{K}(k_x),\hat{K}(-k_x)]. \tag{9}$$

Here, $\hat{K}=\hat{H}-\mu\hat{n}$ is the grand canonical Hamiltonian and $\hat{A}(\vec{k})=\Sigma\exp(i\vec{k}\cdot\vec{r})\hat{A}(\vec{r})$ is the Fourier decomposition for mode k of a local operator $\hat{A}(\vec{r})$ which operates at position $\vec{r}$. It should be noted that the heat and charge currents are related via the energy current as $\hat{J}_x^Q=\hat{J}_x^E-(\mu/q_e)\hat{J}_x$ with

TABLE I. Broadening factor η for the t-J model on a two-dimensional triangular lattice with $\mathcal{L}=12$ sites. Both positive and negative values of the hopping t are given. The value of J has very little effect on η compared to the weak x dependence.

x	$\eta/\lvert t\rvert(J=0.2\lvert t\rvert,t>0)$	$\eta/\lvert t\rvert(J=0,t<0)$
0.83	3.229589	2.678842
0.75	4.198734	4.221241
0.67	4.659046	4.697231
0.58	4.922330	4.934004
0.17	3.786627	3.772738
0.083	2.803789	2.769104

$$\hat{J}_x^E=-\lim_{k_x\to 0}\frac{d}{dk_x}\left[\hat{T}(k_x),\frac{1}{2}\hat{T}(-k_x)+\hat{U}(-k_x)\right], \tag{10}$$

with $\hat{T}$ and $\hat{U}$ being equal to the kinetic and potential energy operators,[21] respectively.

From Refs. 8–10, the definitions for stress tensor $\hat{\tau}_{xx}$, the thermoelectric operator $\hat{\Phi}_{xx}$, and the thermal operator $\hat{\Theta}_{xx}$ are

$$\hat{\tau}_{xx}=-\lim_{k_x\to 0}\frac{d}{dk_x}[\hat{J}_x(k_x),q_e\hat{n}(-k_x)], \tag{11}$$

$$\hat{\Phi}_{xx}=-\lim_{k_x\to 0}\frac{d}{dk_x}[\hat{J}_x(k_x),\hat{K}(-k_x)], \tag{12}$$

$$\hat{\Theta}_{xx}=-\lim_{k_x\to 0}\frac{d}{dk_x}[\hat{J}_x^Q(k_x),\hat{K}(-k_x)]. \tag{13}$$

The explicit forms of these operators for the t-J model are given in the Appendix.

Throughout this work, we take the chemical potential $\mu(T)$ in the above formulas to be that obtained from the canonical ensemble, i.e., $\mu(T)=\partial F/\partial N$, where $F=-(1/\beta)\ln(\mathcal{Z})$ is the Helmholtz free energy. For a finite sized system, we approximate this partial derivative as $\mu(T)=(F_{N+1}-F_{N-1})/2$ for an N electron system.[22]

When calculating the full frequency dependent conductivities for finite sized clusters, one must take into account the discreteness of the energy spectrum caused by the finite nature of the cluster. This is done by introducing a broadening factor η where the frequency then becomes $\omega_c\to\omega+i\eta$. The broadening factor is taken to be the mean energy spacing between states with nonzero current matrix elements. Table I provides values of η for the systems considered here and η is generally weakly dependent on x and of order $\eta\sim 3|t|$.

Following the work of Refs. 8–10, one can consider the high frequency limit of the thermopower, Lorenz number, and figure of merit in the hope and expectation that for strongly correlated systems modeled by the t-J model, these combinations of conductivities will have weak frequency dependence and yet still capture the essential strongly correlated physics, i.e., the Mott-Hubbard physics. For notational convenience, we indicate the high frequency expansions by an asterisk, that is,

$$S^*(T) = \lim_{w\to\infty} S(\omega,T) = \frac{\langle\hat{\Phi}_{xx}\rangle}{T\langle\hat{\tau}_{xx}\rangle}, \tag{14}$$

$$L^*(T) = \lim_{w\to\infty} L(\omega,T) = \frac{\langle\hat{\Theta}_{xx}\rangle}{T^2\langle\hat{\tau}_{xx}\rangle} - \{S^*(T)\}^2, \tag{15}$$

and

$$Z^*(T)T = \lim_{w\to\infty} Z(\omega,T)T = \frac{\{S^*(T)\}^2}{L^*(T)}. \tag{16}$$

While the high frequency quantities with asterisk are not trivial to calculate, they are considerably simpler than the full dynamical Kubo formulas [Eqs. (2)–(4)] as they are equilibrium expectation values and not dynamical in nature. It is also reasonable to expect that in the future, approximate methods could be used to calculate their full temperature dependence that are not as limited as the exact diagonalization brute force methods used here. However, one must be very careful when aiming to establish new approximation for strongly correlated systems and, hence, the need for the brute force calculations in this work.

IV. THERMOPOWER

The thermopower can be factored instructively[12] as

$$S(\omega,T) = \frac{\gamma(\omega,T)}{\sigma(\omega,T)} = \frac{\tilde{\gamma}(\omega,T)}{\sigma(\omega,T)} - \frac{\mu(T)}{q_eT}, \tag{17}$$

where $\gamma(\omega,T)=\tilde{\gamma}(\omega,T)-[\mu(T)/q_eT]\sigma(\omega,T)$ defines $\tilde{\gamma}(\omega,T)$. This factorization displays clearly the two contributions composing the thermopower; one arising from electron transport and the other from thermodynamics (entropy). This is discussed in detail below.

As was mentioned previously, calculating this type of formula for strongly correlated systems is very difficult. Often, there is a desire to give the transport term little importance and, therefore, drop it. This leaves merely the second term in Eq. (17) involving the chemical potential alone. This is the so-called Mott-Heikes (MH) term for the thermopower which is valid at high temperatures and is described in more detail below. However, as will be shown below, for low to intermediate temperatures, this approximation is not adequate.

On physical as well as theoretical[23] grounds, one expects the thermopower to vanish at $T=0$, and for a noninteracting system, it is simple to show this. For our purposes, it is instructive to describe this vanishing through a delicate balancing act where the transport term exactly equals the MH term as the temperature tends toward zero, i.e.,

$$\lim_{T\to 0}\left\{\frac{\tilde{\gamma}(\omega,T)}{\sigma(\omega,T)} - \frac{\mu(T)}{q_eT}\right\} = 0. \tag{18}$$

Achieving this balance in a finite sized system is not possible explicitly, even for noninteracting electrons. However, it does suggest a formulation of the thermopower into the two contributing terms mentioned above: a frequency dependent transport term $S_{tr}(\omega,T)$ and a frequency independent MH term $S_{MH}(T)$ both defined through

$$S(\omega,T) = \frac{1}{T}\left\{\frac{T\tilde{\gamma}(\omega,T)}{\sigma(\omega,T)} - \frac{T\tilde{\gamma}(\omega,0)}{\sigma(\omega,0)}\right\} - \left\{\frac{\mu(T)-\mu(0)}{q_eT}\right\}$$
$$= S_{tr}(\omega,T) + S_{MH}(T). \tag{19}$$

Therefore, even for a finite sized system, one can obtain a transport term and a MH term that independently equal zero at $T=0$, ensuring that $S(\omega,T)$ vanishes in the zero temperature limit as expected. This is not the complete picture, however. The MH term contains the chemical potential which is expected to behave quadratically in T as $T\to 0$ for thermodynamically large systems. Finite systems have two particular differences. One is that the spectrum is discrete, giving rise to a ground state energy gap in situations without degeneracies. In those instances, there will be a low temperature exponential behavior of $\mu(T)$ which is not really a problem for our purposes because $\mu(T)/T$ will still vanish in the zero temperature limit. The existence of ground state degeneracies, on the other hand, is a bigger concern. Their existence causes the chemical potential to behave linearly in T at low temperatures which, in turn, produces a MH term that does not vanish. We argue that this is an unwanted unphysical result and our solution is to merely discount this ground state degeneracy (when it exists) when calculating $\mu(T)$, ensuring that the MH term vanishes as $T\to 0$.

The high frequency expansion of $S(\omega,T)$ is similarly written as

$$S^*(T) = \frac{1}{T}\left\{\frac{\langle\hat{\tilde{\Phi}}_{xx}(T)\rangle}{\langle\tau_{xx}(T)\rangle} - \frac{\langle\hat{\tilde{\Phi}}_{xx}(0)\rangle}{\langle\tau_{xx}(0)\rangle}\right\} + S_{MH}(T)$$
$$= S^*_{tr}(T) + S_{MH}(T). \tag{20}$$

Again, we have defined $\hat{\tilde{\Phi}}_{xx}$ similarly to $\tilde{\gamma}(\omega,T)$ through $\hat{\Phi}_{xx}=\hat{\tilde{\Phi}}_{xx}-[\mu(T)/q_e]\hat{\tau}_{xx}$.

The transport term of the thermopower eventually vanishes as T becomes large so we know that the Mott-Heikes term eventually dominates the thermopower and becomes useful for a number of reasons. One reason is that it is not a dynamical quantity and, hence, is easier to compute. Second, it is often hoped that the MH term dominates the thermopower and one only needs to consider it. This is due to the fact that at high temperatures, it approaches a constant since $\mu(T)$ is eventually linear in T. Previous work by Beni[24] and Chaikin and Beni[25] worked out the infinite temperature limit of $S_{MH}(T)$ for a number of systems. There is elegance and simplicity to these formulas since the infinite temperature limit of $S_{MH}(T)$ is determined merely from counting arguments related to the Hilbert space dimension of the problem at hand. A central question regarding the MH term is at how low temperature does the MH limit remain a valid approximation to the full thermopower. We provide an answer to that question for the t-J model in this work which is discussed later.

The two MH limits we consider here are for the uncorrelated band[26] and for the t-J model,[8,25,27]

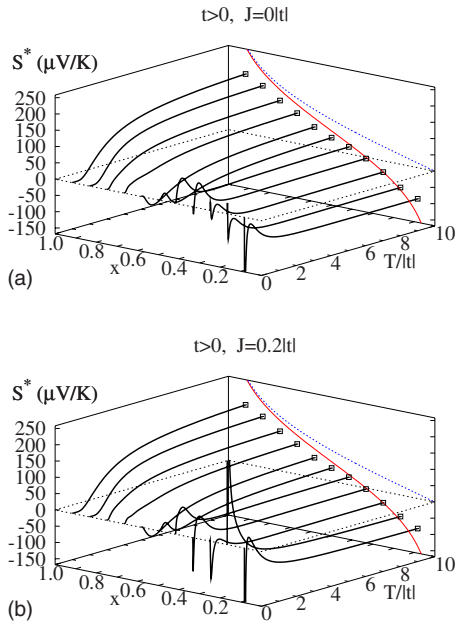

FIG. 2. (Color online) $S^*(T)$ (black curve) as a function of doping x and temperature T for positive hopping $t>0$ corresponding to NCO after particle-hole transformation. Panels (a) and (b) are for $J=0$ and $0.2|t|$, respectively. Projected onto the $T=10|t|$ plane are the Mott-Heikes limits for the uncorrelated [blue (black) dotted] and the t-J models [solid red (gray)], respectively. $S^*(T)$ approaches the MH limit for the t-J model relatively quickly, i.e., by approximately $T\sim 6|t|$. The horizontal black dotted lines indicate the position of zero thermopower.

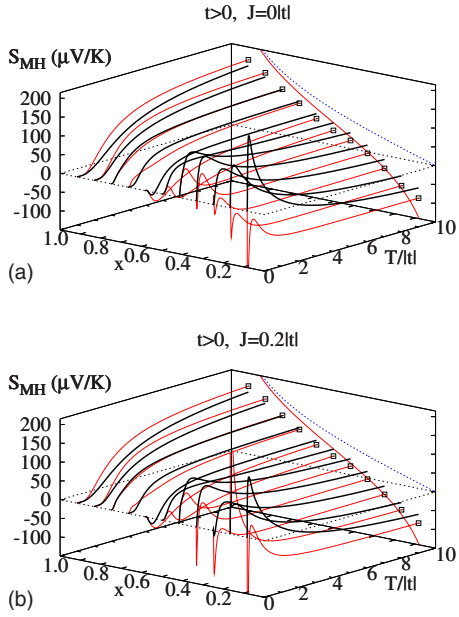

FIG. 3. (Color online) The Mott-Heikes term of the thermopower $S_{MH}(T)$ versus doping x and temperature T for positive hopping $t>0$ corresponding to NCO after particle-hole transformation. Panels (a) and (b) are for $J=0$ and $0.2|t|$, respectively. The black curve is $S_{MH}(T)$, while the red (gray) curve is the full $S^*(T)$. The MH limits are projected onto the $T=10|t|$ plane as in Fig. 2. The horizontal black dotted lines indicate the position of zero thermopower.

$$\lim_{T\to\infty} S_{MH}(T)$$

$$= \begin{cases} \dfrac{k_B}{q_e}\ln\left(\dfrac{2-n}{n}\right), & \text{uncorrelated with } 0\le n\le 2 \\ \dfrac{k_B}{q_e}\ln\left(\dfrac{2(1-n)}{n}\right), & t\text{-}J \text{ with } 0\le n\le 1 \\ -\dfrac{k_B}{q_e}\ln\left(\dfrac{2(n-1)}{2-n}\right), & t\text{-}J \text{ with } 1\le n\le 2, \end{cases} \tag{21}$$

remembering that $q_e=-|e|$ is the electric charge.

Although a somewhat blunt formulation, the Mott-Heikes limits already contain a plethora of information. For example, for the uncorrelated model, even with a finite interaction parameter U, the thermopower diverges at $x\to 1$ ($n\to 0$), is positive for all hole dopings $x>0$ ($n<1$), and is exactly zero for the half filled case $x=0$ ($n=1$). For electron doping, the thermopower would be purely negative, diverging negatively as $x\to 1$ ($n\to 2$). In the whole range of densities ($0\leqslant n\leqslant 2$), the MH limit would predict a single sign change.

For the t-J model, the essentially infinite strength interactions of the electrons cause two additional sign changes compared to the uncorrelated or finite U Hubbard model. The thermopower still diverges as $x\to 1$, is positive for $x>1/3$, is negative for $x<1/3$, and diverges negatively at half filling. For electron doping, we use particle-hole symmetry to get precisely the opposite behavior: a positive divergence at half filling, positive for $x<1/3$, a sign change to negative thermopower for $x>1/3$, and a negative divergence as $x\to 1$. Hence, two additional zero crossings emerge due to the interactions.

In the following sections, we report results for $S^*(T)$, the difference $S(\omega,T)-S^*(T)$, and the Mott-Heikes term $S_{MH}(T)$ for both positive (Sec. IV A) and negative (Sec. IV B) signs of the hopping t. In all figures, the thermopower is given in experimental units of μV/K where $k_B/|q_e|=86$ μV/K, and we have multiplied by (-1) to facilitate comparison with the electron doped NCO system [see Eq. (21)].

A. Positive hopping $t>0$

Figure 2 shows $S^*(T)$ as a function of both doping and temperature for the case of positive hopping $t>0$. We have computed $S^*(T)$ for two different values of J, namely, $J=0$ [Fig. 2(a)] and $J=0.2|t|$ [Fig. 2(b)]. Projected onto the $T=10|t|$ plane are the two MH limits: the uncorrelated model (blue dashed line) and the t-J model (solid red line). The high temperature behavior of $S^*(T)$ matches the t-J model MH limit expectation quite satisfactorily, producing a sign change near $x=1/3$. The slight difference between $S^*(T=10|t|)$ is a combination of $T=10|t|$ being large but finite and

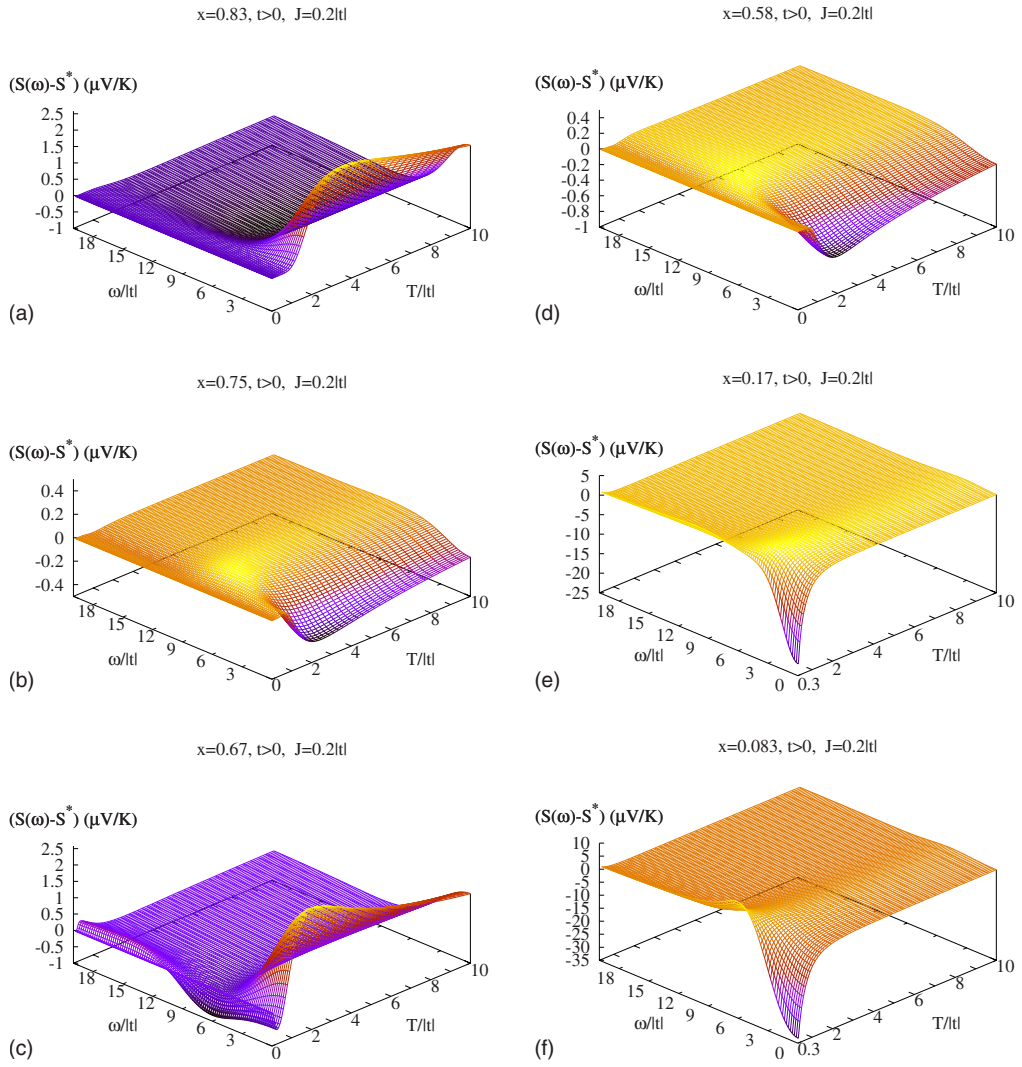

FIG. 4. (Color online) $S(\omega,T)-S^*(T)$ as a function of frequency ω and temperature T for $J=0.2|t|$, positive sign of the hopping $t>0$ (corresponding to NCO after particle-hole transformation), and for dopings (a) $x=0.83$, (b) $x=0.75$, (c) $x=0.67$, (d) $x=0.58$, (e) $x=0.17$, and (f) $x=0.083$. The frequency dependence is evidently quite weak for dopings $x\geqslant 0.58$ [(a)–(d)]. For $x=0.17$ and 0.083 [(e) and (f)], there is a much stronger frequency dependence that occurs at extremely small ω and T. This is most likely due to finite size effects of our $\mathcal{L}=12$ site lattice and not an intrinsic property of the t-J model at these dopings. For parameters $\omega>3|t|$ and $T>2|t|$, the frequency dependence is approximately flat. The doping of $x=0.92$ corresponds in our case to only one electron and, hence, has no frequency dependence.

finite size effects coming from the finite dimension of the Hilbert space, yielding a discrepancy even at $T=\infty$.

For large dopings $x\geqslant 0.58$, the thermopower monotonically grows to a somewhat large value of 100–200 μV/K, growing faster with temperature the higher the doping. The value of J has little to no effect in this range of doping. The thermopower is pinned at zero for $T=0$ and needs to eventually increase to its MH limit which in this range of doping is positive and large. Since the doping is large, there is little interaction between electrons and evidently they effectively avoid one another. Hence, the transport term $S^*_{tr}(T)$ has very little impact on the full thermopower. This physics is borne out by comparing $S^*(T)$ to only the Mott-Heikes term $S_{MH}(T)$ which is shown in Figs. 3(a) and 3(b), where there is very little difference between $S^*(T)$ and $S_{MH}(T)$.

For dopings $x\leqslant 0.5$, strong electron correlation effects are obtained. This is due to the transport term which acts to reduce the thermopower at low to intermediate temperatures. $S^*(T)$ no longer monotonically approaches its MH limit. Again, this is shown more distinctly when one compares $S^*(T)$ to $S_{MH}(T)$ in Figs. 3(a) and 3(b), where the MH term overestimates the thermopower indicative of a very active and important transport term $S^*_{tr}(T)$ which serves to reduce the thermopower. Eventually, the transport term vanishes as T becomes large and the MH term again dominates.

As the doping approaches half filling $(x\rightarrow 0)$, the thermopower begins to be purely negative and nearly monotonically approaches its now negative MH limit. Some of the violent behavior at the lowest temperatures reported is no doubt due to peculiarities of the finite sized lattice. That aside, the transport term has an increasingly important role to play at low to intermediate temperatures as the doping is reduced. Again, this is quite obvious in Figs. 3(a) and 3(b), where the MH and transport terms are quite divergent.

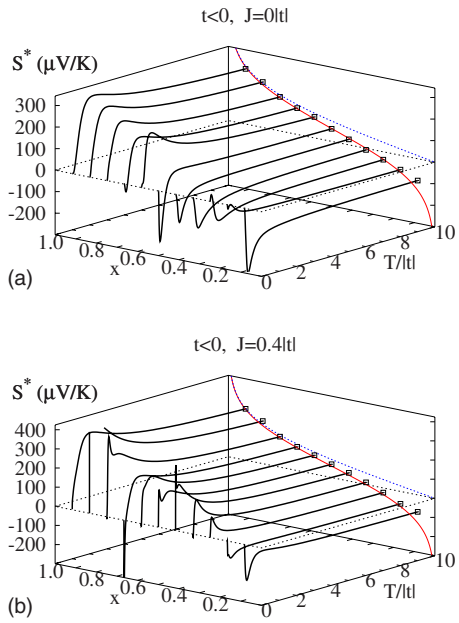

FIG. 5. (Color online) $S^*(T)$ (black curve) as a function of doping x and temperature T for negative hopping $t<0$ corresponding to a fiduciary hole doped CoO_2 compound. Panels (a) and (b) are for $J=0$ and $0.4|t|$, respectively. Projected onto the $T=10|t|$ plane are the MH limits (cf. Fig. 2). $S^*(T)$ approaches the MH limit for the $t-J$ model relatively quickly, i.e., by approximately $T\sim 6|t|$. The horizontal black dotted lines indicate the position of zero thermopower.

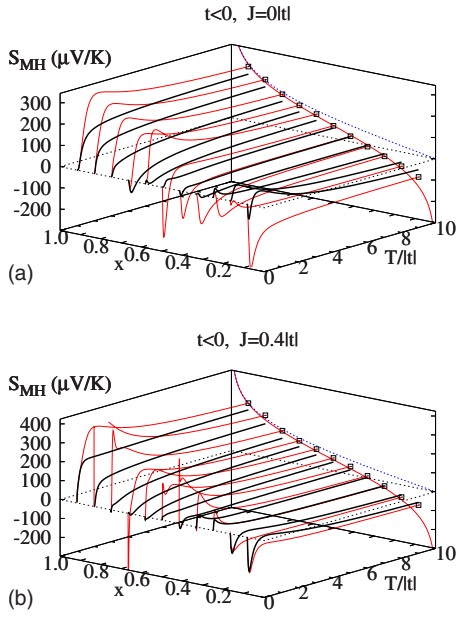

FIG. 6. (Color online) The Mott-Heikes term of the thermopower $S_{MH}(T)$ versus doping x and temperature T for negative hopping $t<0$ corresponding to a fiduciary hole doped CoO_2 compound. Panels (a) and (b) are for $J=0$ and $0.4|t|$, respectively. The black curve is $S_{MH}(T)$, while the red (gray) curve is the full $S^*(T)$. The MH limits are projected onto the $T=10|t|$ plane as in Fig. 2. The horizontal black dotted lines indicate the position of zero thermopower.

Hence, it is definitely not a good approximation to use $S_{MH}(T)$ as a representative of the thermopower in low doping regions of strongly correlated systems for low to intermediate temperatures ($T\leqslant 5|t|$).

The value of J has almost no effect on the thermopower until a doping of $x=0.25$ is reached. Similar results for $J=0.4|t|$ are not shown.

It is interesting to note that $S^*(T)$ can be well approximated by the infinite temperature MH limit for all dopings and all J when the temperature is at or above approximately $5|t|\lesssim T\lesssim 6|t|$, as the thermopower has an overwhelming MH contribution by that temperature.

Last, we justify the use of $S^*(T)$ instead of the full dynamical thermopower $S(\omega,T)$. Figures 4(a)–4(f) show $S(\omega,T)-S^*(T)$ as a function of temperature and frequency ω for dopings $x=0.83$, 0.75, 0.67, 0.58, 0.17, and 0.08. The dopings $x=0.5$, 0.42, 0.33, and 0.25 cannot be calculated at this time due to computational constraints, i.e., the double sum over the current matrix elements in Eqs. (5) and (6) is quite prohibitive. For $x\geqslant 0.58$, the difference between the dynamical thermopower and the infinite frequency expansion is less than 2.5 μV/K and hence has very little absolute effect (approximately less than $\sim 2\%$ difference). Further, it should be noted that for values of $\omega>3|t|$ and temperatures $T>2|t|$, the frequency dependence of the thermopower is nearly nonexistent.

For smaller dopings, i.e., $x=0.17$ and 0.083, a more severe difference between $S(\omega,T)$ and $S^*(T)$ is found. However, this larger difference takes place at extremely small frequencies and temperatures especially considering that this calculation is done for a finite sized system. Recall from Fig. 2(b) that at temperatures below approximately $T\sim 0.3|t|$, the thermopower displays a drastic behavior as it approaches $T=0$. This extreme behavior is almost certainly a consequence of the finite sized lattice on which we work and not an intrinsic property of the $t-J$ model. In fact, in Figs. 4(e) and 4(f), we have cut the temperature off below $T=0.3|t|$ as the thermopower is badly divergent. Therefore, it should be concluded that the frequency dependence of $S(\omega,T)$ is most likely weak even for very small dopings.

B. Negative hopping $t<0$

We now consider the thermopower for a fiduciary system where we have switched the sign of the hopping t, i.e., $t<0$. Since we study $0\leqslant n\leqslant 1$, by a particle-hole transformation, this corresponds to $t>0$ for $1\leqslant n\leqslant 2$, which differs from Na_xCoO_2 in the sign of the hopping ($t<0$ for NCO). Such a system does not exist in the laboratories, and our hope is that our result will stimulate the search for a hole doped CoO_2 system.

In view of the topology of the geometrically frustrated triangular lattice, there is the possibility of important effects coming from primarily the transport term. In Ref. 8, Shastry obtained a high temperature expansion of $S^*(T)$ for the triangular lattice which we quote here for completeness for the situation corresponding to $0\leqslant n\leqslant 1$ and $t>0$,

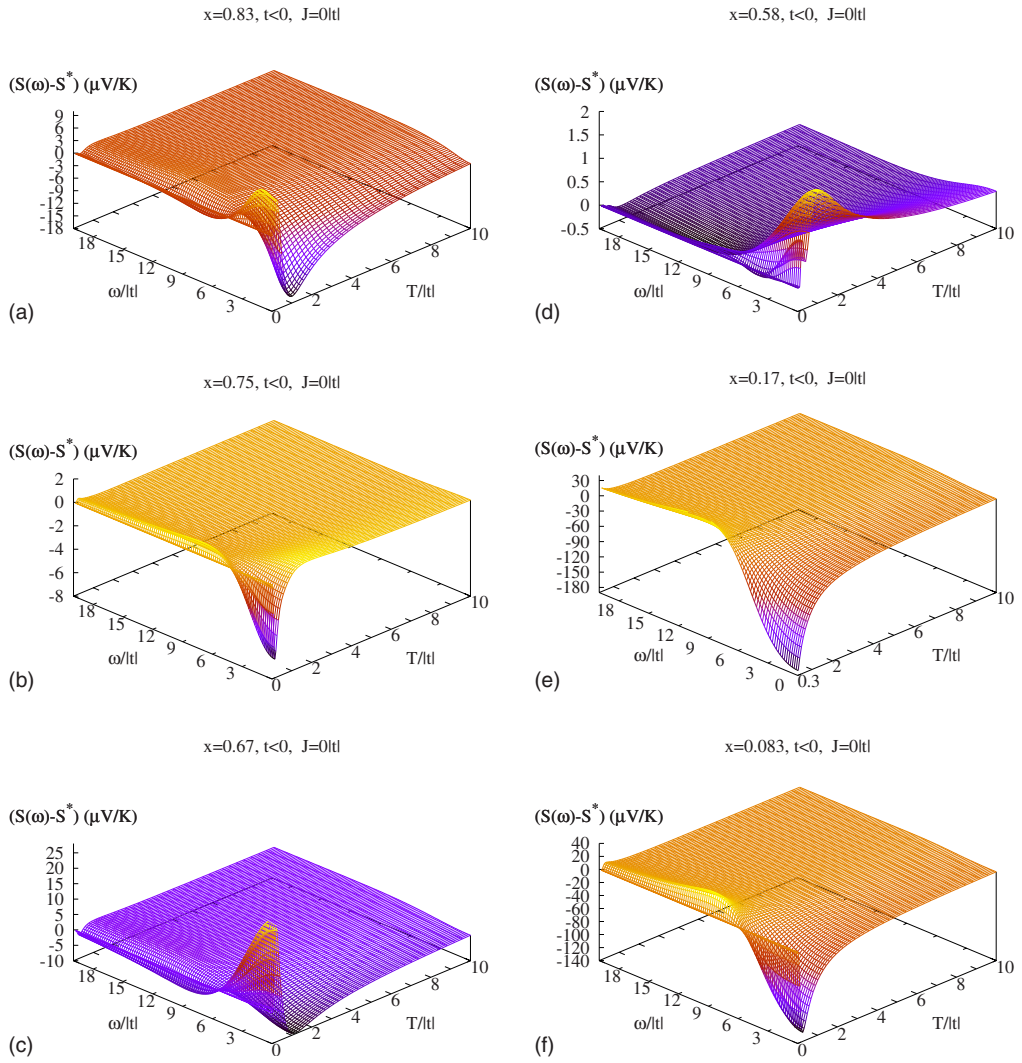

FIG. 7. (Color online) $S(\omega,T)-S^*(T)$ as a function of frequency ω and temperature T for $J=0$, negative sign on the hopping $t<0$ (corresponding to a fiduciary hole doped CoO_2 compound), and dopings (a) $x=0.83$, (b) $x=0.75$, (c) $x=0.67$, (d) $x=0.58$, (e) $x=0.17$, and (f) $x=0.083$. The general frequency dependence is quite similar, albeit larger (discussed further in the text), to that shown in Fig. 4 for positive hopping.

$$S^*(T) = \frac{k_B}{q_e}\left\{\ln\left(\frac{2x}{1-x}\right) - t\frac{1+x}{2T}\right\} + \mathcal{O}(\beta^2 t^2), \qquad (22)$$

with hole doping $x=1-n$. Comparison with an electron doped system such as NCO is facilitated through the particle-hole transformation given previously (see Sec. II). The first term in Eq. (22) is the Mott-Heikes term. The second term is due to the transport and serves to reduce the thermopower from its large MH upper limit as the temperature is decreased. Importantly, it depends on a single power of the hopping t. Hence, if one could switch the sign of the hopping, then $S^*(T)$ would evidently grow to a maximum as the temperature was decreased before approaching its zero value at $T=0$. A term similar to the second term in Eq. (22) with an odd power of t is only present in cases where the topology of the underlying lattice is geometrically frustrated.

Figures 5(a) and 5(b) show $S^*(T)$ for the case of negative hopping as a function of x and T for $J=0$ and $J=0.4|t|$, respectively [recall that we actually plot $(-1)\times S^*(T)$ to facilitate comparison with NCO]. The prediction of thermopower enhancement is quite clearly visible. For dopings $x>0.5$, instead of monotonically decreasing from its upper MH limit, the thermopower grows to a maximum at approximately $1|t| \lesssim T \lesssim 2|t|$ before being pinned by its $T=0$ constraint. The enhancement is also larger for larger dopings. Again, the value of J has little effect other than at extremely low temperatures which most assuredly suffer from finite size effects. As expected, the thermopower obtains its MH limit when T reaches $5|t| \lesssim T \lesssim 6|t|$ just as for the positive hopping situation.

The origin of the thermopower enhancement stems from the transport term $S^*_{tr}(T)$ as expected. Figures 6(a) and 6(b) show the Mott-Heikes formula for the thermopower along

with the full $S^*(T)$ for the negative hopping case. The MH term clearly underestimates the magnitude of the enhancement and nearly misses it all together. Obviously, the transport term has a much more sensitive dependence on the lattice topology than the MH term.

The magnitude of the enhancement is also quite striking. A value of thermopower greater than 150 μV/K is already anomalously large for a seemingly metallic system such as this. However, upon switching the sign of the hopping parameter, a value of the thermopower of nearly 350 μV/K is obtained. Clearly, one should consider the intermediate temperature transport effects when attempting to discover and /or design large thermopower materials; for NCO [$|t| \sim 100$ K (Refs. 8, 9, 12, and 13)], the intermediate temperature range corresponds to approximately room temperature.

The intermediate temperature enhancement of the thermopower is very similar in magnitude and shape to the enhanced thermopower of NCO at high dopings observed recently by Lee *et al.*[28] Although there is, at present, no reason to believe that the experimental system has an inversion of the sign of the hopping as the doping is increased from the Curie-Weiss metallic phase, the similarity between our calculation and the data is striking.

For completeness, Figs. 7(a) and 7(f) display the full frequency dependence of $S(\omega,T)$ compared to $S^*(T)$ for the negative hopping. The same general behavior is shown compared to the positive hopping situation in Figs. 4(a)–4(f). The main difference between the two cases is that the deviation of $S(\omega,T)$ and $S^*(T)$ is slightly more extreme. However, similarly, this is seen to occur at low temperatures, frequencies, and dopings, and is most likely a finite size artifact.

V. LORENZ NUMBER

The Lorenz number is an important thermoelectric quantity, and no less important is its role in the dimensionless figure of merit (FOM). The FOM is an extremely important quantity when determining the technological usefulness and performance of a thermoelectric material where values of FOM in excess of unity are highly desirable.

Recall the definition of the Lorenz number from Eq. (3),

$$L(\omega,T) = \frac{\kappa(\omega,T)}{T\sigma(\omega,T)} - S(\omega,T)^2, \tag{23}$$

which can be simplified as

$$L(\omega,T) = \frac{\tilde{\kappa}(\omega,T)}{T\sigma(\omega,T)} - \left\{\frac{\tilde{\gamma}(\omega,T)}{\sigma(\omega,T)}\right\}^2, \tag{24}$$

with $\kappa(\omega,T) = \tilde{\kappa}(\omega,T) - [2\mu(T)/q_e]\tilde{\gamma}(\omega,T) + [\mu(T)/\sqrt{T}q_e]^2 \times \sigma(\omega,T)$ being used to define $\tilde{\kappa}(\omega,T)$. The chemical potential drops out of this formula entirely; hence, one could calculate $L(\omega,T)$ in a purely canonical ensemble. For noninteracting electrons, it is easy to show that at $T=0$, the Lorenz number is equal to $L_0 = (\pi k_B/\sqrt{3}q_e)^2$. This result is simply the familiar Wiedemann-Franz law (see Refs. 4 and 29). The way this number is obtained in the noninteracting case via our formalism is that at $T=0$, there is a delicate balance similar to that in the thermopower, namely,

$$\lim_{T\to 0}\left(T^2\frac{\tilde{\kappa}(\omega,T)}{\sigma(\omega,T)} - \left\{T\frac{\tilde{\gamma}(\omega,0)}{\sigma(\omega,0)}\right\}^2\right) = 0. \tag{25}$$

The value of L_0 comes from the temperature dependence of both terms. As $T\to 0$, both $\tilde{\kappa}(\omega,T)/T\sigma(\omega,T)$ and $[\tilde{\gamma}(\omega,T)/\sigma(\omega,T)]^2$ behave quadratically in temperature and the difference in the coefficients multiplying each quadratic term is equal precisely to L_0.

In our finite sized system, we have neither the delicate balance of the $T=0$ behavior nor the quadratic low temperature behavior present. Using the same "trick" as we used for the thermopower, we force each term to separately vanish at $T=0$, i.e.,

$$L(\omega,T) = \frac{1}{T^2}\left\{\frac{T\tilde{\kappa}(\omega,T)}{\sigma(\omega,T)} - \frac{T\tilde{\kappa}(\omega,0)}{\sigma(\omega,0)}\right\} - \frac{1}{T^2}\left\{\left(\frac{T\tilde{\gamma}(\omega,T)}{\sigma(\omega,T)}\right)^2 - \left(\frac{T\tilde{\gamma}(\omega,0)}{\sigma(\omega,0)}\right)^2\right\}, \tag{26}$$

to keep $L(\omega,T)$ from badly diverging. At low temperatures, the exponential behavior caused by the discrete nature of the energy levels of the finite system rears its head causing problems as $T\to 0$.

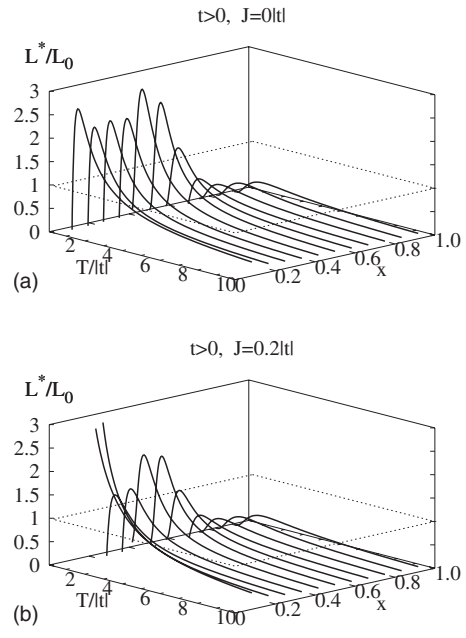

FIG. 8. $L^*(T)/L_0$ (black curve) as a function of doping x and temperature T for positive hopping $t>0$ (corresponding to NCO after a particle-hole transformation) where $L_0=(\pi k_B/\sqrt{3}q_e)^2$. Panels (a) and (b) are for $J=0$ and $0.2|t|$, respectively. The horizontal black dotted lines indicate $L^*(T)/L_0=1$.

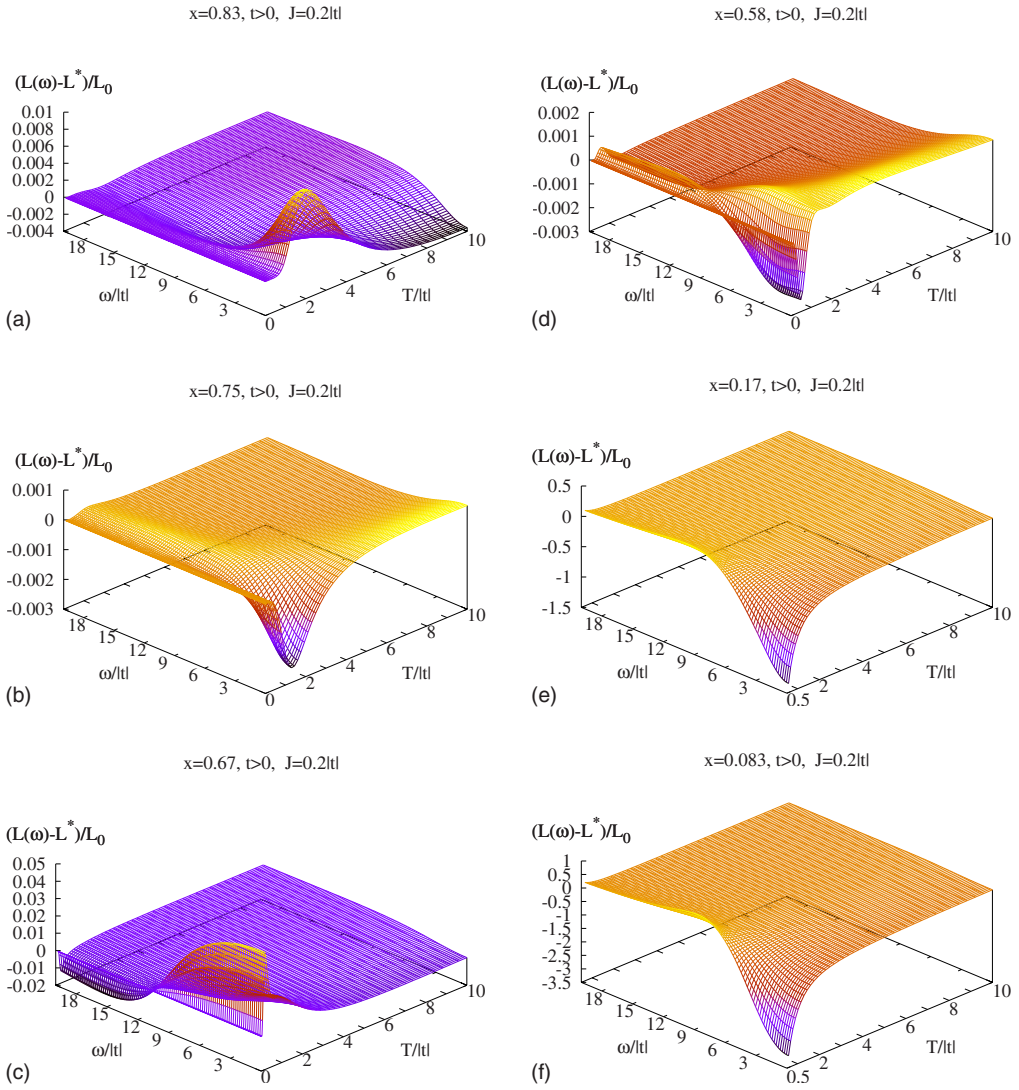

FIG. 9. (Color online) $(L(\omega,T)-L^*(T))/L_0$ as a function of frequency ω and temperature T for $J=0.2|t|$, positive hopping $t>0$ (corresponding to NCO after a particle-hole transformation), and dopings (a) $x=0.83$, (b) $x=0.75$, (c) $x=0.67$, (d) $x=0.58$, (e) $x=0.17$, and (f) $x=0.083$. The frequency dependence is weak for dopings $x\geqslant 0.58$ [(a)–(d)]. For $x=0.17$ and 0.083 [(e) and (f)], there is strong dependence occurring at small ω and T. Note that in (e) and (f), we are only considering temperatures $T\geqslant 0.5|t|$ as the Lorenz number badly diverges below that temperature. This is most likely a finite size effect and not an intrinsic property of the t-J model at these dopings.

At present, we are only able to consider a couple of issues regarding the Lorenz number. First, we can still quite satisfactorily determine the accuracy of using the high frequency expansion of $L^*(T)$ in place of $L(\omega,T)$. Second, we can determine generally qualitative aspects of the Lorenz number for strongly correlated systems as a function of both temperature and doping. Our qualitative determination of $L(\omega,T)$ also allows us to look at the dimensionless figure of merit which we investigate in Sec. VI again at a qualitative level.

The high frequency expansion of $L(\omega,T)$ is

$$L^*(T)=\frac{\langle\hat{\tilde{\Theta}}_{xx}\rangle\langle\hat{\tau}_{xx}\rangle-\langle\hat{\tilde{\Phi}}_{xx}\rangle^2}{T^2\langle\hat{\tau}_{xx}\rangle^2}, \tag{27}$$

where similar to $\tilde{\kappa}(\omega,T)$ we have defined $\hat{\tilde{\Theta}}_{xx}$ through $\hat{\Theta}_{xx}=\hat{\tilde{\Theta}}_{xx}-[2\mu(T)/q_e]\hat{\tilde{\Phi}}_{xx}+[\mu(T)/q_e]^2\hat{\tau}_{xx}$. After forcing each term to vanish at $T=0$, Eq. (27) becomes

$$L^*(T)=\frac{1}{T^2}\left\{\frac{\langle\hat{\tilde{\Theta}}_{xx}(T)\rangle}{\langle\tau_{xx}(T)\rangle}-\frac{\langle\hat{\tilde{\Theta}}_{xx}(0)\rangle}{\langle\tau_{xx}(0)\rangle}\right\}-\frac{1}{T^2}\left\{\frac{\langle\hat{\tilde{\Phi}}_{xx}(T)\rangle^2}{\langle\tau_{xx}(T)\rangle^2}-\frac{\langle\hat{\tilde{\Phi}}_{xx}(0)\rangle^2}{\langle\tau_{xx}(0)\rangle^2}\right\}. \tag{28}$$

In Figs. 8(a), 8(b), and 9(a)–9(f), we report results for $L^*(T)/L_0$ and $[L(\omega,T)-L^*(T)]/L_0$ for the case of the

hopping relevant to NCO. The dotted black line in Figs. 8(a) and 8(b) is to indicate unity. It is a reasonable assumption that at $T=0$, a thermodynamically large system would have a finite value of $L^*(T)$ at $T=0$. Whether this finite value is equal to L_0 is an open question and one we are unfortunately not able to shed light upon at this time.

For the noninteracting case, the behavior of $L^*(T)$ quickly deviates from L_0 where it is pinned at $T=0$ as a function of temperature. For the interacting case shown here, the Lorenz number quickly decays to very small values as T increases as well. However, our results indicate that the intermediate temperature behavior of $L^*(T)$ generally grows with decreasing doping x, i.e., interactions evidently increase the Lorenz number. The effect of J is much harder to discern due to presumably finite size effects and low temperature divergences. J seems to have little effect except for the highest dopings calculated $x=0.17$ and 0.083.

Figure 9 is similar to Figs. 4 and 7. For dopings $x \geqslant 0.58$, the frequency dependence of $L(\omega,T)$ is very weak and only on the order of $\sim(2-3)\%$ or less. At the low dopings of $x=0.17$ and 0.083, there is again a much stronger frequency dependence that is likely due to finite size effects and not intrinsic to the t-J model.

With confidence in the weak frequency dependence of the thermopower and the Lorenz number, we proceed to calculate the dimensionless FOM for the situation applicable to NCO.

VI. FIGURE OF MERIT

A value of the dimensionless figure of merit greater than 1 is indicative of a good thermoelectric material and is therefore desired. Of course, throughout this work, we have neglected the lattice contribution to the Lorenz number which will add to our calculation of $L(\omega,T)$ and consequently serve to decrease the FOM that we calculate below.

Recall that the FOM is given in Eq. (4), while the high frequency expansion is given by Eq. (16). The numerator is just the square of the thermopower and vanishes at zero temperature and eventually obtains the square of the MH limit, i.e., $\{(86\ \mu\mathrm{V/K})\ln[2x/(1-x)]\}^2$. However, the denominator is the Lorenz number which starts out finite at $T=0$ and quickly decays to zero as $T\to\infty$. Therefore, we expect the FOM to begin at zero and grow without bound as T increases.

Figures 10(a) and 10(b) show the FOM for $J=0$ and $J=0.2|t|$ for the positive case of the hopping t as a function of both the doping and temperature. True to expectations, the FOM quickly grows from zero at $T=0$ to well above unity for dopings $x \geqslant 0.58$. At intermediate dopings ($0.5 \geqslant x \geqslant 0.17$), the FOM remains very small up to the largest temperatures calculated and never reaches unity. This is understandable when one considers that the thermopower in this regime has a small absolute value for all temperatures and the Lorenz number only serves to diminish this value. At the smallest doping calculated ($x=0.083$), the FOM just reaches unity as $T\sim 10|t|$.

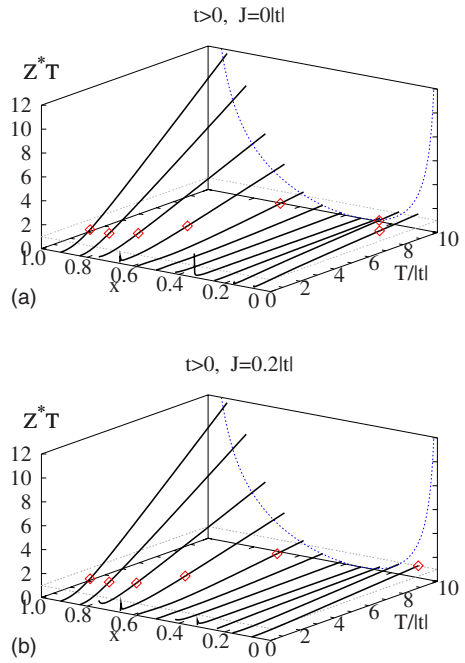

FIG. 10. (Color online) $Z^*(T)T$ (black curve) as a function of doping x and temperature T for (a) $J=0$ and (b) $0.2|t|$. The red (gray) squares indicate the point at which $Z^*(T)T=1$, while the black dotted line indicates unity as well. Projected onto the $T=10|t|$ plane is the "normalized" square of the MH term, i.e., $\{\ln[2x/(1-x)]\}^2$ [blue (black) dotted curve].

Note that in Fig. 10 we have indicated the point at which $Z^*(T)T$ equals 1 by a red box. Projected onto the $T=10|t|$ plane is the "normalized" square of the MH term, i.e., $\{\ln[2x/(1-x)]\}^2$, indicating an interesting doping behavior of the relative magnitudes of the figure of merit. This behavior is most certainly due to the MH term of the thermopower. Nonzero J has a nearly negligible effect except at the lowest dopings where it serves to slightly reduce the highest temperature value of the FOM.

The full frequency dependence of $Z(\omega,T)T$ is understandably weak (not shown) since both the thermopower and Lorenz number have been shown to be weakly frequency dependent.

VII. CONCLUSION

In this work, we have established the general validity of the high frequency expansion of the thermopower, Lorenz number, and figure of merit for strongly correlated electron models. This high frequency expansion is much simpler to consider than the full Kubo formalism and yet complicated enough to capture the full interaction effects. This established validity should provide a benchmark encouraging the theoretical community to obtain useful approximate methods to calculate these high frequency formulas.

We also provide theoretical evidence supporting the authors' previous calculations in regard to the Curie-Weiss

metallic phase of NCO[12,13] being qualitatively and quantitatively described by a two-dimensional t-J model on a triangular lattice. Further, we have provided predictions for sodium cobalt oxide concerning the Lorenz number and figure of merit (Secs. V and VI). In Refs. 12 and 13, the present authors used an experimental hopping parameter of $|t| \sim 100$ K taken from both photoemission experiments[30,31] and chemical potential measurements,[32] indicating NCO to have a very narrow band system. Therefore, one should scale the temperature in this work by this value of the hopping when making experimental comparisons.

The predicted thermopower enhancement discussed in Sec. IV B should stimulate an experimental search of lattice based strongly correlated materials to provide useful thermolectric materials. Perhaps, it is possible to custom design a high thermopower material armed with the knowledge of the behavior of the transport term alone for strongly correlated systems.

ACKNOWLEDGMENTS

We gratefully acknowledge support from Grant No. NSF-DMR0408247 and DOE BES Grant No. DE-FG02-06ER46319. We also thank J. B. Anderson (Chemistry) and Eric Prescott (Computer Science and Engineering) at the Pennsylvania State University for allowing time on the computer cluster MUFASA which is supported by CEMBA, an NSF funded IGERT program. We also acknowledge enlightening conversations with Subroto Mukerjee.

APPENDIX: OPERATOR EXPRESSIONS

This appendix presents formulas taken from Refs. 8–10 for completeness and clarity and additional ones used in the present work.

In discussing the explicit forms of the operators, we introduce the so-called Hubbard operators to act to simplify the formulas somewhat. The Hubbard operators are defined as follows:

$$X_{\sigma 0}(\vec{r}) \equiv \tilde{c}^{\dagger}_{\vec{r}\sigma}, \tag{A1}$$

$$X_{0\sigma}(\vec{r}) \equiv \tilde{c}_{\vec{r}\sigma}, \tag{A2}$$

$$X_{\sigma\sigma'}(\vec{r}) \equiv \tilde{c}^{\dagger}_{\vec{r}\sigma}\tilde{c}_{\vec{r}\sigma'} = X_{\sigma 0}(\vec{r}')X_{0\sigma'}(\vec{r}'), \tag{A3}$$

$$X_{00}(\vec{r}) \equiv \tilde{c}_{\vec{r}\sigma}\tilde{c}^{\dagger}_{\vec{r}\sigma} = X_{0\sigma}(\vec{r})X_{\sigma 0}(\vec{r}). \tag{A4}$$

They have modified anticommutation relations

$$\{\tilde{c}^{\dagger}_{\vec{r}\sigma}, \tilde{c}_{\vec{r}\sigma'}\} = [X_{\sigma 0}(\vec{r}), X_{0\sigma}(\vec{r}')] = \delta_{\vec{r}\vec{r}'}[X_{\sigma\sigma'}(\vec{r}) + \delta_{\sigma\sigma'}X_{00}(\vec{r})]$$
$$\equiv \delta_{\vec{r}\vec{r}'}Y_{\sigma'\sigma}(\vec{r}'), \tag{A5}$$

where the last line defines $Y_{\sigma'\sigma}(\vec{r})$. Using this notation, the charge and energy currents defined in Eqs. (8) and (10) are given by

$$\hat{J}_x = -\lim_{k_x\to 0}\frac{d}{dk_x}[\hat{K}(k_x), q_e\hat{n}(-k_x)] = iq_e t\sum_{r\eta\sigma}\eta_x X_{\sigma 0}(\vec{r}+\vec{\eta})X_{0\sigma}(\vec{r}) \tag{A6}$$

and

$$\hat{J}^E_x = -\lim_{k_x\to 0}\frac{d}{dk_x}\left[\hat{T}(k_x), \frac{1}{2}\hat{T}(-k_x) + \hat{U}(-k_x)\right] = -\frac{it^2}{2}\sum_{r\eta\eta'\sigma\sigma'}(\eta_x+\eta'_x)Y_{\sigma\sigma'}(\vec{r}+\vec{\eta})X_{\sigma 0}(\vec{r}+\vec{\eta}+\vec{\eta}')X_{0\sigma'}(\vec{r}) + \frac{iJt}{4}\sum_{r\eta\eta'\sigma}\{\eta_x\vec{\mu}(\vec{r}$$
$$+\vec{\eta},\vec{r})\cdot(\vec{S}_{\vec{r}+\vec{\eta}'} + \vec{S}_{\vec{r}+\vec{\eta}+\vec{\eta}'}) + [(\eta_x+2\eta'_x)\vec{S}_{\vec{r}+\vec{\eta}+\vec{\eta}'} + (\eta_x-2\eta'_x)\vec{S}_{\vec{r}+\vec{\eta}'}]\cdot\vec{\mu}(\vec{r}+\vec{\eta},\vec{r})\}, \tag{A7}$$

respectively.

The stress tensor is simply

$$\hat{\tau}_{xx} = -\lim_{k_x\to 0}\frac{d}{dk_x}[\hat{J}_x(k_x), \hat{q}_e n(-k_x)] = q_e^2 t\sum_{r\eta\sigma}\eta_x^2 X_{\sigma 0}(\vec{r}+\vec{\eta})X_{0\sigma}(\vec{r}), \tag{A8}$$

while the modified thermoelectric and thermal operators ($\hat{\tilde{\Phi}}_{xx}$ and $\hat{\tilde{\Theta}}_{xx}$) have the form

$$\hat{\tilde{\Phi}}_{xx} = -\lim_{k_x\to 0}\frac{d}{dk_x}[\hat{J}_x(k_x), \hat{H}(-k_x)] = -q_e\frac{t^2}{2}\sum_{r\eta\eta'\sigma\sigma'}(\eta_x+\eta'_x)^2 Y_{\sigma\sigma'}(\vec{r}+\vec{\eta})X_{\sigma 0}(\vec{r}+\vec{\eta}+\vec{\eta}')X_{0\sigma'}(\vec{r}) + \frac{q_e tJ}{4}\sum_{r\eta\eta'\sigma}\{\eta_x[\eta_x\vec{\mu}(\vec{r}$$
$$+\vec{\eta},\vec{r})\cdot(\vec{S}_{\vec{r}+\vec{\eta}'} + \vec{S}_{\vec{r}+\vec{\eta}+\vec{\eta}'}) + [(\eta_x+2\eta'_x)\vec{S}_{\vec{r}+\vec{\eta}+\vec{\eta}'} + (\eta_x-2\eta'_x)\vec{S}_{\vec{r}+\vec{\eta}'}]\cdot\vec{\mu}(\vec{r}+\vec{\eta},\vec{r})\} \tag{A9}$$

and

$$\hat{\tilde{\Theta}}_{xx} = -\lim_{k_x\to 0}\frac{d}{dk_x}[\hat{J}^E_x(k_x),\hat{H}(-k_x)] = \frac{t^3}{4}\sum_{r\eta\eta'\eta''}\Bigg\{\sum_{\sigma}(\eta_x+\eta'_x)(-\eta_x+\eta'_x-\eta''_x)[\{X_{\bar{\sigma}0}(\vec{r}+\vec{\eta})X_{0\sigma}(\vec{r}+\vec{\eta}+\vec{\eta}'')-X_{\bar{\sigma}0}(\vec{r}+\vec{\eta}$$
$$+\vec{\eta}'')X_{0\sigma}(\vec{r}+\vec{\eta})\}X_{\sigma 0}(\vec{r}+\vec{\eta}+\vec{\eta}')X_{0\bar{\sigma}}(\vec{r})-\{X_{\bar{\sigma}0}(\vec{r}+\vec{\eta})X_{0\bar{\sigma}}(\vec{r}+\vec{\eta}+\vec{\eta}'')-\text{h.c.}\}X_{\sigma 0}(\vec{r}+\vec{\eta}+\vec{\eta}'')X_{0\sigma}(\vec{r})]+\sum_{\sigma\sigma'\sigma''}(\eta_x+\eta'_x$$
$$+\eta''_x)(\eta_x+2\eta'_x+\eta''_x)Y_{\sigma\sigma'}(\vec{r}+\vec{\eta})Y_{\sigma''\sigma'}(\vec{r}+\vec{\eta}+\vec{\eta}')X_{\sigma'''0}(\vec{r}+\vec{\eta}+\vec{\eta}'+\vec{\eta}'')X_{0\sigma'}(\vec{r})\Bigg\}+\frac{t^2J}{16}\sum_{r\eta\eta'\eta''}(\eta_x+\eta'_x)\Bigg\{\sum_{\sigma\sigma'}[(\eta_x$$
$$-\eta'_x)X_{\sigma 0}(\vec{r}+\vec{\eta}+\vec{\eta}')X_{0\sigma'}(\vec{r})[X_{\sigma'\bar{\sigma}}(\vec{r}+\vec{\eta})X_{\bar{\sigma}\sigma}(\vec{r}+\vec{\eta}+\vec{\eta}'')-X_{\bar{\sigma}\sigma}(\vec{r}+\vec{\eta})X_{\sigma'\bar{\sigma}}(\vec{r}+\vec{\eta}+\vec{\eta}'')]-(\eta_x+\eta'_x)Y_{\sigma\sigma'}(\vec{r}+\vec{\eta})X_{\bar{\sigma}0}(\vec{r}$$
$$+\vec{\eta}+\vec{\eta}')X_{0\sigma'}(\vec{r})X_{\sigma\bar{\sigma}}(\vec{r}+\vec{\eta}+\vec{\eta}'+\vec{\eta}'')-(\eta_x+\eta'_x)Y_{\sigma\sigma'}(\vec{r}+\vec{\eta})X_{\sigma 0}(\vec{r}+\vec{\eta}+\vec{\eta}')X_{0\bar{\sigma}}(\vec{r})X_{\bar{\sigma}\sigma}(\vec{r}+\vec{\eta}'')+(\eta_x-\eta'_x+2\eta''_x)$$
$$\times[X_{\bar{\sigma}\sigma}(\vec{r}+\vec{\eta}+\vec{\eta}'')X_{\sigma'\bar{\sigma}}(\vec{r}+\vec{\eta})-X_{\sigma'\bar{\sigma}}(\vec{r}+\vec{\eta}+\vec{\eta}'')X_{\bar{\sigma}\sigma}(\vec{r}+\vec{\eta})]X_{\sigma 0}(\vec{r}+\vec{\eta}+\vec{\eta}')X_{0\sigma'}(\vec{r})-(\eta_x+\eta'_x+2\eta''_x)X_{\sigma\bar{\sigma}}(\vec{r}+\vec{\eta}$$
$$+\vec{\eta}'+\vec{\eta}'')Y_{\sigma\sigma'}(\vec{r}+\vec{\eta})X_{\bar{\sigma}0}(\vec{r}+\vec{\eta}+\vec{\eta}')X_{0\sigma'}(\vec{r})-(\eta_x+\eta'_x-2\eta''_x)X_{\bar{\sigma}\sigma'}(\vec{r}+\vec{\eta}'')Y_{\sigma\sigma'}(\vec{r}+\vec{\eta})X_{\sigma 0}(\vec{r}+\vec{\eta}+\vec{\eta}')X_{0\bar{\sigma}}(\vec{r})-(\eta_x$$
$$+\eta'_x-\eta''_x)Y_{\sigma\sigma'}(\vec{r}+\vec{\eta})X_{\sigma 0}(\vec{r}+\vec{\eta}+\vec{\eta}')X_{0\sigma'}(\vec{r})[n_{\vec{r}+\vec{\eta}'\sigma'}-n_{\vec{r}+\vec{\eta}''\bar{\sigma}}]-(\eta_x+\eta'_x+\eta''_x)Y_{\sigma\sigma'}(\vec{r}+\vec{\eta})[n_{\vec{r}+\vec{\eta}+\vec{\eta}'+\vec{\eta}''\sigma}$$
$$-n_{\vec{r}+\vec{\eta}+\vec{\eta}'+\vec{\eta}''\bar{\sigma}}]X_{\sigma 0}(\vec{r}+\vec{\eta}+\vec{\eta}')X_{0\sigma'}(\vec{r})]+(2\eta_x-2\eta'_x+2\eta''_x)\sum_{\sigma}[n_{\vec{r}+\vec{\eta}+\vec{\eta}''\sigma}-n_{\vec{r}+\vec{\eta}+\vec{\eta}''\bar{\sigma}}]X_{\bar{\sigma}\sigma}(\vec{r}+\vec{\eta})X_{\sigma 0}(\vec{r}+\vec{\eta}+\vec{\eta}')X_{0\bar{\sigma}}(\vec{r})\Bigg\}$$
$$+\frac{tJ^2}{8}\sum_{r\eta\eta'\eta''}\Bigg\{\sum_{\alpha\beta\gamma}i\epsilon_{\alpha\beta\gamma}\Bigg[\eta_x\mu^{\alpha}(\vec{r}+\vec{\eta},\vec{r})\Bigg\{S^{\beta}_{\vec{r}+\vec{\eta}''}\Bigg[\frac{\eta_x}{4}S^{\gamma}_{\vec{r}+\vec{\eta}''}-\frac{\eta_x}{4}S^{\gamma}_{\vec{r}+\vec{\eta}+\vec{\eta}''}-\frac{(\eta_x-2\eta'_x)}{2}S^{\gamma}_{\vec{r}+\vec{\eta}+\vec{\eta}'}\Bigg]+S^{\beta}_{\vec{r}+\vec{\eta}+\vec{\eta}'}\Bigg[\frac{\eta_x}{4}S^{\gamma}_{\vec{r}+\vec{\eta}''}$$
$$-\frac{\eta_x}{4}S^{\gamma}_{\vec{r}+\vec{\eta}+\vec{\eta}''}+\frac{(\eta_x+2\eta'_x)}{2}S^{\gamma}_{\vec{r}+\vec{\eta}+\vec{\eta}'+\vec{\eta}''}\Bigg]\Bigg\}+\eta_x\Bigg[\frac{(\eta_x-2\eta''_x)}{4}S^{\alpha}_{\vec{r}+\vec{\eta}''}-\frac{(\eta_x+2\eta''_x)}{4}S^{\alpha}_{\vec{r}+\vec{\eta}+\vec{\eta}''}-\frac{(\eta_x-2\eta'_x-2\eta''_x)}{2}S^{\alpha}_{\vec{r}+\vec{\eta}+\vec{\eta}''}\Bigg]\mu^{\beta}(\vec{r}$$
$$+\vec{\eta},\vec{r})S^{\gamma}_{\vec{r}+\vec{\eta}}+\eta_x\Bigg[\frac{(\eta_x-2\eta''_x)}{4}S^{\alpha}_{\vec{r}+\vec{\eta}''}-\frac{(\eta_x+2\eta''_x)}{4}S^{\alpha}_{\vec{r}+\vec{\eta}+\vec{\eta}''}+\frac{(\eta_x+2\eta'_x+2\eta''_x)}{2}S^{\alpha}_{\vec{r}+\vec{\eta}+\vec{\eta}'+\vec{\eta}''}\Bigg]\mu^{\beta}(\vec{r}+\vec{\eta},\vec{r})S^{\gamma}_{\vec{r}+\vec{\eta}+\vec{\eta}'}+(\eta_x+2\eta'_x)$$
$$\times\Bigg[S^{\alpha}_{\vec{r}+\vec{\eta}+\vec{\eta}'}\mu^{\beta}(\vec{r}+\vec{\eta},\vec{r})\Bigg\{\frac{\eta_x}{4}S^{\gamma}_{\vec{r}+\vec{\eta}+\vec{\eta}''}-\frac{\eta_x}{4}S^{\gamma}_{\vec{r}+\vec{\eta}''}-\frac{(\eta_x+2\eta'_x)}{2}S^{\gamma}_{\vec{r}+\vec{\eta}+\vec{\eta}'+\vec{\eta}''}\Bigg\}+\Bigg\{\frac{(\eta_x+2\eta''_x)}{4}S^{\alpha}_{\vec{r}+\vec{\eta}+\vec{\eta}''}-\frac{(\eta_x-2\eta''_x)}{4}S^{\alpha}_{\vec{r}+\vec{\eta}''}$$
$$-\frac{(\eta_x+2\eta'_x+2\eta''_x)}{2}S^{\alpha}_{\vec{r}+\vec{\eta}+\vec{\eta}'+\vec{\eta}''}\Bigg\}S^{\beta}_{\vec{r}+\vec{\eta}+\vec{\eta}'}\mu^{\gamma}(\vec{r}+\vec{\eta},\vec{r})\Bigg]+(\eta_x-2\eta''_x)\Bigg[S^{\alpha}_{\vec{r}+\vec{\eta}'}\mu^{\beta}(\vec{r}+\vec{\eta},\vec{r})\Bigg\{\frac{\eta_x}{4}S^{\gamma}_{\vec{r}+\vec{\eta}+\vec{\eta}''}-\frac{\eta_x}{4}S^{\gamma}_{\vec{r}+\vec{\eta}''}$$
$$+\frac{(\eta_x-2\eta'_x)}{2}S^{\gamma}_{\vec{r}+\vec{\eta}+\vec{\eta}''}\Bigg\}+\Bigg\{\frac{(\eta_x+2\eta''_x)}{4}S^{\alpha}_{\vec{r}+\vec{\eta}+\vec{\eta}''}-\frac{(\eta_x-2\eta''_x)}{4}S^{\alpha}_{\vec{r}+\vec{\eta}''}+\frac{(\eta_x-2\eta'_x-2\eta''_x)}{2}S^{\alpha}_{\vec{r}+\vec{\eta}+\vec{\eta}''}\Bigg\}S^{\beta}_{\vec{r}+\vec{\eta}'}\mu^{\gamma}(\vec{r}+\vec{\eta},\vec{r})\Bigg]\Bigg]$$
$$+\sum_{\alpha}\Bigg[\frac{\eta_x^2}{8}X_{\sigma 0}(\vec{r}+\vec{\eta})X_{0\sigma}(\vec{r})\{S^{\alpha}_{\vec{r}+\vec{\eta}'}+S^{\alpha}_{\vec{r}+\vec{\eta}+\vec{\eta}'}\}\{S^{\alpha}_{\vec{r}+\vec{\eta}''}+S^{\alpha}_{\vec{r}+\vec{\eta}+\vec{\eta}''}\}+\Bigg\{\frac{\eta_x(\eta_x-2\eta''_x)}{8}S^{\alpha}_{\vec{r}+\vec{\eta}''}+\frac{\eta_x(\eta_x+2\eta''_x)}{8}S^{\alpha}_{\vec{r}+\vec{\eta}+\vec{\eta}''}\Bigg\}X_{\sigma 0}(\vec{r}$$
$$+\vec{\eta})X_{0\sigma}(\vec{r})\{S^{\alpha}_{\vec{r}+\vec{\eta}'}+S^{\alpha}_{\vec{r}+\vec{\eta}+\vec{\eta}'}\}+\frac{(\eta_x+2\eta'_x)}{8}\{S^{\alpha}_{\vec{r}+\vec{\eta}+\vec{\eta}'}X_{\sigma 0}(\vec{r}+\vec{\eta})X_{0\sigma}(\vec{r})[\eta_xS^{\alpha}_{\vec{r}+\vec{\eta}''}+\eta_xS^{\alpha}_{\vec{r}+\vec{\eta}+\vec{\eta}''}]+[(\eta_x-2\eta''_x)S^{\alpha}_{\vec{r}+\vec{\eta}''}+(\eta_x$$
$$+2\eta''_x)S^{\alpha}_{\vec{r}+\vec{\eta}+\vec{\eta}''}]S^{\alpha}_{\vec{r}+\vec{\eta}+\vec{\eta}'}X_{\sigma 0}(\vec{r}+\vec{\eta})X_{0\sigma}(\vec{r})\}+\frac{(\eta_x-2\eta'_x)}{8}\{S^{\alpha}_{\vec{r}+\vec{\eta}'}X_{\sigma 0}(\vec{r}+\vec{\eta})X_{0\sigma}(\vec{r})[\eta_xS^{\alpha}_{\vec{r}+\vec{\eta}''}+\eta_xS^{\alpha}_{\vec{r}+\vec{\eta}+\vec{\eta}''}]+[(\eta_x-2\eta''_x)S^{\alpha}_{\vec{r}+\vec{\eta}''}$$
$$+(\eta_x+2\eta''_x)S^{\alpha}_{\vec{r}+\vec{\eta}+\vec{\eta}''}]S^{\alpha}_{\vec{r}+\vec{\eta}'}X_{\sigma 0}(\vec{r}+\vec{\eta})X_{0\sigma}(\vec{r})\}\Bigg]\Bigg\}, \tag{A10}$$

respectively. In the above expression for $\hat{\tilde{\Phi}}_{xx}$ and $\hat{\tilde{\Theta}}_{xx}$, we have used the bond spin operators defined as

$$\mu^z(\vec{r},\vec{r}') = \frac{1}{2}[X_{\uparrow 0}(\vec{r})X_{0\uparrow}(\vec{r}')-X_{\downarrow 0}(\vec{r})X_{0\downarrow}(\vec{r}')], \tag{A11}$$

$$\mu^y(\vec{r},\vec{r}') = \frac{1}{2i}[X_{\uparrow 0}(\vec{r})X_{0\downarrow}(\vec{r}')-X_{\downarrow 0}(\vec{r})X_{0\uparrow}(\vec{r}')], \tag{A12}$$

$$\mu^x(\vec{r},\vec{r}') = \frac{1}{2}[X_{\uparrow 0}(\vec{r})X_{0\downarrow}(\vec{r}')+X_{\downarrow 0}(\vec{r})X_{0\uparrow}(\vec{r}')]. \tag{A13}$$

Further, note that for Eq. (A10), we have used the definition

$$\hat{J}_x^E(k_x) = -\lim_{q_x\to 0}\frac{d}{dq_x}\left\{\frac{1}{2}[\hat{T}(q_x+k_x),\hat{T}(-q_x)] + [\hat{T}(q_x+k_x),\hat{V}(-q_x)]\right\} \quad \text{(A14)}$$

allowing the establishment of the identity (using the Jacobi identity)

$$\lim_{k_x,q_x\to 0}\frac{d^2}{dk_x dq_x}\left\{[[\hat{T}(k_x+q_x),\hat{V}(-q_x)],\hat{T}(-k_x)] - \frac{1}{2}[[\hat{T}(k_x+q_x),\hat{T}(-q_x)],\hat{V}(-k_x)]\right\} = 0, \quad \text{(A15)}$$

simplifying the calculation of Eq. (A10) tremendously.

*peterson@physics.ucsc.edu

[1] I. Terasaki, Y. Sasago, and K. Uchinokura, Phys. Rev. B **56**, R12685 (1997).
[2] B. G. Levi, Phys. Today **56**(8), 15 (2003).
[3] Y. Y. Wang, N. S. Rogado, R. J. Cava, and N. P. Ong, Nature (London) **423**, 425 (2003).
[4] J. M. Ziman, *Principles of the Theory of Solids* (Cambridge University Press, Cambridge, 1979).
[5] R. Kubo, J. Phys. Soc. Jpn. **12**, 570 (1957).
[6] G. D. Mahan, *Many-particle Physics* (Plenum, New York, 1990).
[7] G. D. Mahan, in *Solid State Physics*, edited by H. Ehrenreich and F. Spaepen (Academic, New York, 1998), Vol. 51, p. 81.
[8] B. S. Shastry, Phys. Rev. B **73**, 085117 (2006); URL http://physics.ucsc.edu/~ sriram/papers_all/ksumrule_errors_etc/evolving.pdf
[9] B. S. Shastry, Phys. Rev. B **74**, 039901(E) (2006).
[10] B. S. Shastry (unpublished).
[11] B. S. Shastry, B. I. Shraiman, and R. R. P. Singh, Phys. Rev. Lett. **70**, 2004 (1993).
[12] J. O. Haerter, M. R. Peterson, and B. S. Shastry, Phys. Rev. Lett. **97**, 226402 (2006).
[13] J. O. Haerter, M. R. Peterson, and B. S. Shastry, Phys. Rev. B **74**, 245118 (2006).
[14] A. P. Ramirez, in *More Is Different*, edited by N. P. Ong and R. N. Bhatt (Princeton University Press, New Jersey, 2001), p. 255.
[15] B. Kumar and B. S. Shastry, Phys. Rev. B **68**, 104508 (2003).
[16] G. Baskaran, Phys. Rev. Lett. **91**, 097003 (2003).
[17] Q.-H. Wang, D.-H. Lee, and P. A. Lee, Phys. Rev. B **69**, 092504 (2004).
[18] J. Jaklic and P. Prelovsek, Adv. Phys. **49**, 1 (2000).
[19] G. Kotliar and D. Vollhardt, Phys. Today **63**(3), 53 (2004).
[20] M. R. Peterson and B. S. Shastry (unpublished).
[21] That is, the Hamiltonian is written as $\hat{H}=\hat{T}+\hat{U}$ where $\hat{T}=-\Sigma_{\vec{r}\vec{\eta}\sigma}t(\vec{\eta})\tilde{c}^{\dagger}_{\vec{r}+\vec{\eta}\sigma}\tilde{c}_{\vec{r}\sigma}$ and $\hat{U}=\frac{1}{2}\Sigma_{\vec{r}\vec{\eta}}J(\vec{\eta})\vec{S}_{\vec{r}}\cdot\vec{S}_{\vec{r}+\vec{\eta}}$.
[22] For a t-J model with $\mathcal{L}$ sites, the possible number of electrons is $N=1,\ldots,\mathcal{L}-1$. So, while $\mu(T)=(F_{N+1}-F_{N-1})/2$ is used for $N=2,\ldots,\mathcal{L}-2$, we define it as $\mu(T)=F_{N+1}-F_N$ for $N=2$ and $\mu(T)=F_N-F_{N-1}$ for $N=\mathcal{L}-1$.
[23] C. A. Stafford, Phys. Rev. B **48**, 8430 (1993).
[24] G. Beni, Phys. Rev. B **10**, 2186 (1974).
[25] P. M. Chaikin and G. Beni, Phys. Rev. B **13**, 647 (1976).
[26] It should be said that the Mott-Heikes limit for an uncorrelated band of spinful particles is equivalent to that of the Hubbard model for arbitrary U. When the $T\to\infty$ limit is taken, the value of U is essentially scaled to zero compared to the temperature yielding the same result as that for an uncorrelated band.
[27] S. Mukerjee and J. E. Moore, Appl. Phys. Lett. **90**, 112107 (2007).
[28] M. Lee, L. Viciu, L. Li, Y. Wang, M. L. Foo, S. Watauchi, R. A. Pascal, Jr., R. J. Cava, and N. P. Ong, Nat. Mater. **5**, 537 (2006).
[29] N. W. Ashcroft and D. N. Mermin, *Solid State Physics* (Brooks-Cole, Belmont, MA, 1976).
[30] M. Z. Hasan *et al.*, Phys. Rev. Lett. **92**, 246402 (2004).
[31] H.-B. Yang *et al.*, Phys. Rev. Lett. **95**, 146401 (2005).
[32] Y. Ishida, H. Ohta, A. Fujimori, and H. Hosono, arXiv:cond-mat/0511149 (unpublished).